

# A Good Long Look at the Black Hole Candidates LMC X-1 and LMC X-3

M. A. Nowak<sup>1</sup>, J. Wilms<sup>2</sup>, W. A. Heindl<sup>3</sup>, K. Pottschmidt<sup>2</sup>, J. B. Dove<sup>4,5</sup>,  
M. C. Begelman<sup>1,6</sup>

<sup>1</sup> *JILA, University of Colorado, Campus Box 440, Boulder, CO 80309-0440, U.S.A.; mnowak@rocinate.colorado.edu*

<sup>2</sup> *Institut für Astronomie und Astrophysik, Abt. Astronomie, Waldhäuser Str. 64, D-72076 Tübingen, Germany; wilms@astro.uni-tuebingen.de, katja@astro.uni-tuebingen.de*

<sup>3</sup> *Center for Astronomy and Space Sciences, University of California at San Diego, La Jolla, CA 92093, U.S.A.; wheindl@mamacass.ucsd.edu*

<sup>4</sup> *Center for Astronomy and Space Astrophysics, University of Colorado, Boulder, CO 80309-389, U.S.A.; dove@casa.colorado.edu*

<sup>5</sup> *also, Dept. of Physics, Metropolitan State College of Denver, C.B. 69, P.O. Box 173362, Denver, CO 80217-3362, U.S.A.*

<sup>6</sup> *also, Dept. of Astrophysics and Planetary Sciences, University of Colorado, Boulder 80309, U.S.A.; mitch@jila.colorado.edu*

Accepted 2000 ; Received 2000; in original form

## ABSTRACT

LMC X-1 and LMC X-3 are the only known persistent stellar-mass black hole candidates that have almost always shown spectra that are dominated by a soft, thermal component. We present here results from 170 ksec long Rossi X-ray Timing Explorer (*RXTE*) observations of these objects, taken in 1996 December, where their spectra can be described by a disc black body plus an additional soft ( $\Gamma \sim 2.8$ ) high-energy power-law (detected up to energies of 50 keV in LMC X-3). These observations, as well as archival Advanced Satellite for Cosmology and Astrophysics (*ASCA*) observations, constrain any narrow Fe line present in the spectra to have an equivalent width  $\lesssim 90$  eV. Stronger, broad lines ( $\approx 150$  eV EW,  $\sigma \approx 1$  keV) are permitted. We also study the variability of LMC X-1. Its X-ray power spectral density (PSD) is approximately  $\propto f^{-1}$  between  $10^{-3}$  and 0.3 Hz with a root mean square (rms) variability of  $\approx 7\%$ . At energies  $> 5$  keV the PSD shows evidence of a break at  $f > 0.2$  Hz, possibly indicating an outer disc radius of  $\lesssim 1000 GM/c^2$  in this likely wind-fed system. Furthermore, the coherence function  $\gamma^2(f)$ , a measure of the degree of linear correlation, between variability in the  $> 5$  keV band and variability in the lower energy bands is extremely low ( $\lesssim 50\%$ ). We discuss the implications of these observations for the mechanisms that might be producing the soft and hard X-rays in these systems.

**Key words:** accretion — black hole physics — Stars: binaries — X-rays:Stars

## 1 INTRODUCTION

Since the discovery of Cygnus X-1 in 1964 (Bowyer et al. 1965), the study of galactic black hole candidates (BHCs) has shown that these objects display a large variety of states which are characterized by their distinct spectral shapes and temporal behaviours. The most important states which have been identified are the “low/hard state”, which is characterized by a hard X-ray spectrum with a photon index  $\Gamma = 1.7$  and large root mean square (rms) variability  $\gtrsim 30\%$  (Tanaka & Lewin 1995; Nowak 1995; and references therein), and the “high/soft state”, which is spectrally softer ( $\Gamma \sim 2.5$ ) and exhibits less variability. The fractional Eddington luminosity of sources in the soft state tends to be higher than that for sources in the hard state (Nowak 1995, and references therein).

The soft state has been observed in steady sources such as LMC X-1 and LMC X-3 (Treves et al. 1988; Ebisawa et al. 1989; Treves et al. 1990; Ebisawa et al. 1993; Schmidtke et al. 1999), in recurring transients such as GX 339–4 (Grebenev et al. 1993), and in a number of transients such as Nova Muscae (Miyamoto et al. 1994). The persistent BHC Cygnus X-1 has been observed to switch between the hard and the soft state (albeit with  $kT \sim 0.3$  keV for the soft state), with the total X-ray luminosity staying roughly constant (Cui et al. 1997; Zhang et al. 1997).

A great deal of observational attention has been focused on the more commonly observed hard state, since most of the brighter galactic BHCs only occasionally transit to the soft state. Only two of the persistent nearby BHCs, LMC X-1 and LMC X-3, until recently have always been observed in the soft state. Wilms et al. (1999d), hereafter Paper II,

present evidence that LMC X-3 periodically transits into the low/hard state. In this work we present 170 ksec long Rossi X-ray Timing Explorer (*RXTE*) observations of both LMC X-1 and LMC X-3 during high/soft X-ray states.

LMC X-3 is a highly variable BHC with a probable  $9 M_{\odot}$  compact object mass (Cowley et al. 1983). Its luminosity has been observed to be as high as  $4 \times 10^{38} \text{ erg s}^{-1}$ , which is  $\approx 30\%$  of its Eddington luminosity, and its soft X-ray flux ( $\sim 1\text{--}9 \text{ keV}$ ) is variable by a factor of more than four on long time scales (see Paper II). LMC X-3 also has exhibited a strong 99- or 198-day periodicity in its soft X-ray flux (Cowley et al. 1991; Cowley et al. 1994), which is also apparent in the *ASM* monitoring, albeit with a period that varies over time (Paper II). Previously we had suggested that this periodicity might be associated with a warped, precessing accretion disc (Wilms et al. 1999b); however, with the recently observed “state changes” to a low/hard flux it now seems likely that a systematic variation of the accretion rate is an important part of this long-term variability.

LMC X-1 is also a good candidate for a black hole. Using a large number of *ROSAT* HRI observations, Cowley et al. (1995) were able to identify the counterpart with “star number 32” of Cowley et al. (1978). This object has a mass function of only  $f = 0.144 M_{\odot}$ , but including other evidence the mass of the compact object appears to be  $M > 4 M_{\odot}$  (Hutchings et al. 1987), and probably  $\gtrsim 6 M_{\odot}$  (Cowley et al. 1995). The luminosity of the object is typically about  $2 \times 10^{38} \text{ erg s}^{-1}$  (Long et al. 1981). Although small differences between LMC X-1 and LMC X-3 are apparent, their spectra and short-time temporal behaviours have historically been quite similar. LMC X-1, however, does not exhibit any obvious periodic behaviour in its long term X-ray lightcurve.

We have monitored LMC X-1 and LMC X-3 with *RXTE* in three to four weekly intervals since the end of 1996 in order to enable a systematic study of the soft state. The campaign started with 170 ksec long observations of both sources, and in this paper we present results from the spectral and temporal analysis of these long observations. In addition, we consider spectral results of archival Advanced Satellite for Cosmology and Astrophysics (*ASCA*) observations. Preliminary results of our analyses have already appeared elsewhere (Wilms et al. 1999b; Wilms et al. 1999c). Results from the monitoring observations are presented in Paper II.

The remainder of this paper is structured as follows. We start with a description of our *RXTE* data analysis methodology (§2). We then present the results from the spectral analysis from *RXTE* (§3) and *ASCA* (§4). The *RXTE* timing analysis is discussed in section 5. We discuss our results in the context of current physical models for the soft state (§6) and then summarize the paper (§7).

## 2 RXTE DATA ANALYSIS METHODS

Onboard *RXTE* are two pointed instruments, the Proportional Counter Array (*PCA*) and the High Energy X-ray Timing Experiment (*HEXTE*), as well as the All Sky Monitor (*ASM*). We used the standard *RXTE* data analysis software, *ftools* 4.2. Spectral modeling was performed mostly with *XSPEC*, version 10.00z (Arnaud 1996). We used essentially the same data extraction and analysis strategy as in

our analyses of *RXTE* data from GX 339–4 and V1408 Aql (4U1957+11); therefore, we only present a brief summary of this strategy. For detailed information we refer to Wilms et al. (1999a) and Nowak & Wilms (1999).

The *PCA* consists of five co-aligned Xenon (with an upper Propane layer) proportional counter units (PCUs) with a total effective area of about  $6500 \text{ cm}^2$ . The instrument is sensitive in the energy range from 2 keV to  $\sim 100 \text{ keV}$  (Jahoda et al. 1996), although the response matrix is best calibrated in the energy range of  $\approx 2.5\text{--}30 \text{ keV}$ . We chose to increase the signal to noise ratio of our data by analyzing top Xenon layer data only. Background subtraction of the *PCA* data was performed analogously to our previous study of Cyg X-1 (Dove et al. 1998). To reduce the uncertainty of the *PCA* background model, we ignored data measured in the 30 minutes after South Atlantic Anomaly (SAA) passages. The *XSPEC* ‘corrfile’ facility was used to renormalize the background file for all observations, typically by 1–2%.

For short ( $\lesssim 10 \text{ ks}$ ) segments of observations, we assumed the uncertainty of the data to be purely from a Poisson distribution. For analysis of the full ( $> 100 \text{ ks}$ ) observations, we accounted for the remaining detector calibration uncertainty by using the energy dependent systematic errors described by Wilms et al. (1999a).

*HEXTE* consists of two clusters of four NaI/CsI-phoswich scintillation counters that are sensitive from 15 to 250 keV. A full description of the instrument is given by Rothschild et al. (1998). Background subtraction is done by source-background switching. We used the standard *HEXTE* response matrices of 1999 August, and considered data measured above 20 keV.

## 3 RXTE SPECTRAL ANALYSIS

### 3.1 LMC X-3

*RXTE* observed LMC X-3 during three observing blocks on 1996 November 30, 1996 December 2, and 1996 December 4 and 5. A log of the observations can be found in Table 1. During part of the observations, some detectors were turned off; however, we added all good data together and combined all background models. The total response matrix was the average of the respective estimates for each individual detector combination, weighted by the fraction of photons measured during the time that such a combination was active.

The lightcurve of LMC X-3 during the long observation is displayed in Fig. 1. During the first part of the observation the source is characterized by a slight increase of the *PCA* count rate from  $\sim 80$  to  $\sim 85 \text{ cps}$  per PCU. The source was at a relatively steady level of  $\sim 77 \text{ cps}$  per PCU during the last part of the observations. This variation was also observed in the *HEXTE* (Fig. 1). To see whether this variation was also detectable spectroscopically, we first analyzed separately the observations indicated in Table 1. For this analysis, we ignored data below *PCA* channel 7 and above *PCA* channel 50, which corresponds to an energy bandpass from 3.6–20 keV. (Here and throughout our spectral discussions, *PCA* channel number refers to the ‘standard\_2f’ channels, 1–129, as read by *XSPEC*.)

We first modeled the spectrum via the standard multi-temperature disc black body (Mitsuda et al. 1984) plus a

**Table 1.** Observing log for the long RXTE observation of LMC X-3.

Obs.	JD-2450000	Date ymd	Exposure sec	Count Rate counts s <sup>-1</sup>
a	417.905	1996.11.30, 09:43	13800	399.3 ± 0.2
b	418.238	1996.11.30, 17:42	10200	412.9 ± 0.2
c	419.843	1996.12.02, 08:14	14000	422.3 ± 0.2
d	420.168	1996.12.02, 16:02	12700	411.3 ± 0.2
e	421.818	1996.12.04, 07:38	12400	369.9 ± 0.2
f	422.100	1996.12.04, 14:25	11300	388.8 ± 0.2
g	422.374	1996.12.04, 20:58	5500	384.2 ± 0.3
h	422.660	1996.12.05, 03:50	16900	374.2 ± 0.2
i	422.960	1996.12.05, 11:02	11300	334.9 ± 0.2
j	423.238	1996.12.05, 17:42	16400	395.0 ± 0.2
k	423.502	1996.12.06, 00:02	15200	392.2 ± 0.2

Exposure times shown are rounded to the closest 100 sec. The count rate is the total PCA background subtracted count rate.

**Table 2.** Results of Spectral Fitting to the LMC X-3 Data.

Obs.	$kT_{\text{in}}$ keV	$A_{\text{disc}}$	$A_{\text{compps}}$ 10 <sup>-2</sup>	$\Gamma$	$A_{\text{PL}}$ 10 <sup>-1</sup>	$kT_{\text{e}}$ keV	$y_{\text{compps}}$ 10 <sup>-2</sup>	$A_{\text{Line}}$ 10 <sup>-4</sup>	EW eV	$\chi^2/\text{dof}$
total	1.24 <sup>+0.00</sup> <sub>-0.01</sub>	33.6 <sup>+0.9</sup> <sub>-0.9</sub>	...	2.0 <sup>+0.1</sup> <sub>-0.2</sub>	2.4 <sup>+1.1</sup> <sub>-0.8</sub>	...	...	0.6 <sup>+0.5</sup> <sub>-0.6</sub>	10	50.4/47
total <sup>a</sup>	1.20 <sup>+0.01</sup> <sub>-0.02</sub>	37.3 <sup>+1.8</sup> <sub>-1.4</sub>	...	2.6 <sup>+0.2</sup> <sub>-0.3</sub>	1.2 <sup>+0.7</sup> <sub>-0.6</sub>	...	...	8.1 <sup>+3.5</sup> <sub>-3.8</sub>	134	37.8/46
a	1.23 <sup>+0.00</sup> <sub>-0.00</sub>	25.6 <sup>+0.6</sup> <sub>-0.6</sub>	...	2.9 <sup>+0.0</sup> <sub>-0.0</sub>	4.8 <sup>+0.4</sup> <sub>-0.3</sub>	...	...	14.1 <sup>+2.9</sup> <sub>-3.7</sub>	22	68.1/39
b	1.24 <sup>+0.00</sup> <sub>-0.00</sub>	28.2 <sup>+0.6</sup> <sub>-0.7</sub>	...	2.9 <sup>+0.0</sup> <sub>-0.0</sub>	3.7 <sup>+0.4</sup> <sub>-0.4</sub>	...	...	1.6 <sup>+0.4</sup> <sub>-0.4</sub>	24	66.6/39
c	1.25 <sup>+0.00</sup> <sub>-0.00</sub>	29.9 <sup>+0.6</sup> <sub>-0.6</sub>	...	3.0 <sup>+0.0</sup> <sub>-0.0</sub>	3.8 <sup>+0.4</sup> <sub>-0.4</sub>	...	...	2.0 <sup>+0.3</sup> <sub>-0.3</sub>	30	99.6/39
d	1.25 <sup>+0.00</sup> <sub>-0.00</sub>	29.7 <sup>+0.6</sup> <sub>-0.5</sub>	...	3.3 <sup>+0.1</sup> <sub>-0.1</sub>	5.0 <sup>+0.6</sup> <sub>-0.6</sub>	...	...	1.8 <sup>+0.4</sup> <sub>-0.3</sub>	28	61.8/39
e	1.24 <sup>+0.00</sup> <sub>-0.00</sub>	30.5 <sup>+0.6</sup> <sub>-0.5</sub>	...	3.4 <sup>+0.1</sup> <sub>-0.1</sub>	4.6 <sup>+0.7</sup> <sub>-0.6</sub>	...	...	1.9 <sup>+0.3</sup> <sub>-0.4</sub>	32	68.6/39
f	1.24 <sup>+0.00</sup> <sub>-0.00</sub>	30.9 <sup>+0.6</sup> <sub>-0.6</sub>	...	3.4 <sup>+0.1</sup> <sub>-0.1</sub>	4.4 <sup>+0.7</sup> <sub>-0.6</sub>	...	...	1.5 <sup>+0.3</sup> <sub>-0.4</sub>	25	59.3/39
g	1.24 <sup>+0.01</sup> <sub>-0.01</sub>	30.5 <sup>+0.8</sup> <sub>-0.5</sub>	...	3.4 <sup>+0.1</sup> <sub>-0.1</sub>	4.4 <sup>+1.1</sup> <sub>-0.9</sub>	...	...	1.6 <sup>+0.5</sup> <sub>-0.5</sub>	28	43.5/39
h	1.23 <sup>+0.00</sup> <sub>-0.00</sub>	30.8 <sup>+0.5</sup> <sub>-0.6</sub>	...	3.3 <sup>+0.1</sup> <sub>-0.1</sub>	4.0 <sup>+0.5</sup> <sub>-0.5</sub>	...	...	1.4 <sup>+0.3</sup> <sub>-0.3</sub>	23	128/39
i	1.23 <sup>+0.00</sup> <sub>-0.00</sub>	30.8 <sup>+0.7</sup> <sub>-0.7</sub>	...	3.1 <sup>+0.1</sup> <sub>-0.1</sub>	3.3 <sup>+0.6</sup> <sub>-0.5</sub>	...	...	1.9 <sup>+0.3</sup> <sub>-0.4</sub>	30	54.5/39
j	1.24 <sup>+0.00</sup> <sub>-0.00</sub>	29.7 <sup>+0.5</sup> <sub>-0.5</sub>	...	3.1 <sup>+0.0</sup> <sub>-0.1</sub>	4.1 <sup>+0.4</sup> <sub>-0.4</sub>	...	...	1.9 <sup>+0.3</sup> <sub>-0.3</sub>	31	63.7/39
k	1.24 <sup>+0.00</sup> <sub>-0.00</sub>	28.8 <sup>+0.5</sup> <sub>-0.6</sub>	...	3.2 <sup>+0.0</sup> <sub>-0.1</sub>	4.8 <sup>+0.5</sup> <sub>-0.5</sub>	...	...	1.4 <sup>+0.3</sup> <sub>-0.3</sub>	23	123/39
total <sup>b</sup>	1.16 <sup>+0.04</sup> <sub>-0.02</sub>	...	2.5 <sup>+0.2</sup> <sub>-1.1</sub>	...	...	62 <sup>+34</sup> <sub>-12</sub>	6.1 <sup>+0.1</sup> <sub>-0.2</sub>	10.1 <sup>+3.6</sup> <sub>-4.6</sub>	170	39.5/46
a	1.11 <sup>+0.01</sup> <sub>-0.01</sub>	...	5.6 <sup>+0.4</sup> <sub>-0.1</sub>	...	...	46 <sup>+5</sup> <sub>-3</sub>	9.5 <sup>+0.1</sup> <sub>-0.0</sub>	13.8 <sup>+1.4</sup> <sub>-1.4</sub>	230	57.2/39
b	1.14 <sup>+0.01</sup> <sub>-0.01</sub>	...	4.6 <sup>+0.6</sup> <sub>-0.7</sub>	...	...	48 <sup>+8</sup> <sub>-5</sub>	8.3 <sup>+0.2</sup> <sub>-0.1</sub>	13.5 <sup>+1.7</sup> <sub>-1.7</sub>	213	46.4/39
c	1.16 <sup>+0.01</sup> <sub>-0.01</sub>	...	2.8 <sup>+0.4</sup> <sub>-0.2</sub>	...	...	64 <sup>+14</sup> <sub>-6</sub>	6.9 <sup>+0.2</sup> <sub>-0.1</sub>	14.6 <sup>+1.5</sup> <sub>-1.5</sub>	228	88.7/39
d	1.16 <sup>+0.00</sup> <sub>-0.00</sub>	...	3.3 <sup>+0.1</sup> <sub>-0.4</sub>	...	...	43 <sup>+14</sup> <sub>-5</sub>	5.3 <sup>+0.1</sup> <sub>-0.2</sub>	13.7 <sup>+1.6</sup> <sub>-1.5</sub>	223	71.7/39
e	1.17 <sup>+0.00</sup> <sub>-0.01</sub>	...	1.3 <sup>+0.3</sup> <sub>-0.5</sub>	...	...	84 <sup>+35</sup> <sub>-15</sub>	4.5 <sup>+0.1</sup> <sub>-0.2</sub>	13.1 <sup>+1.5</sup> <sub>-1.6</sub>	228	80.8/39
f	1.16 <sup>+0.00</sup> <sub>-0.00</sub>	...	2.9 <sup>+0.1</sup> <sub>-0.5</sub>	...	...	40 <sup>+11</sup> <sub>-5</sub>	4.3 <sup>+0.1</sup> <sub>-0.1</sub>	11.0 <sup>+1.6</sup> <sub>-2.2</sub>	190	67.9/39
g	1.16 <sup>+0.01</sup> <sub>-0.01</sub>	...	2.1 <sup>+0.3</sup> <sub>-1.0</sub>	...	...	50 <sup>+20</sup> <sub>-10</sub>	4.2 <sup>+0.2</sup> <sub>-0.2</sub>	10.8 <sup>+3.0</sup> <sub>-2.2</sub>	190	57.3/39
h	1.15 <sup>+0.01</sup> <sub>-0.00</sub>	...	2.8 <sup>+0.0</sup> <sub>-0.4</sub>	...	...	44 <sup>+11</sup> <sub>-4</sub>	4.6 <sup>+0.1</sup> <sub>-0.1</sub>	11.4 <sup>+1.3</sup> <sub>-1.3</sub>	202	113/39
i	1.16 <sup>+0.01</sup> <sub>-0.01</sub>	...	1.5 <sup>+0.0</sup> <sub>-0.1</sub>	...	...	89 <sup>+30</sup> <sub>-12</sub>	5.6 <sup>+0.2</sup> <sub>-0.1</sub>	12.2 <sup>+1.7</sup> <sub>-1.7</sub>	213	68.8/39
j	1.16 <sup>+0.00</sup> <sub>-0.01</sub>	...	2.4 <sup>+0.2</sup> <sub>-0.1</sub>	...	...	64 <sup>+15</sup> <sub>-6</sub>	6.0 <sup>+0.1</sup> <sub>-0.1</sub>	12.4 <sup>+1.3</sup> <sub>-1.4</sub>	209	80.1/39
k	1.15 <sup>+0.01</sup> <sub>-0.00</sub>	...	3.1 <sup>+0.2</sup> <sub>-0.1</sub>	...	...	50 <sup>+8</sup> <sub>-6</sub>	5.8 <sup>+0.1</sup> <sub>-0.1</sub>	12.2 <sup>+1.3</sup> <sub>-1.2</sub>	210	130/39

$T_{\text{in}}$ ,  $A_{\text{disc}}$ : Peak multi-temperature disc temperature and normalization.  $\Gamma$ : Photon index of the power law.  $A_{\text{PL}}$ : Power law normalization (photons keV<sup>-1</sup> cm<sup>-2</sup> s<sup>-1</sup> at 1 keV).  $A_{\text{compps}}$ : Normalization of **compps** model.  $kT_{\text{e}}$ : Coronal electron temperature for the **compps** model.  $y_{\text{compps}}$ : Compton y-parameter for the **compps** model.  $A_{\text{Line}}$ : Line normalization (photons cm<sup>-2</sup> s<sup>-1</sup> in the line). The Gaussian line was fixed at 6.4 keV with a width of  $\sigma = 0.1$  keV for the multi-temperature disc plus black body models, or  $\sigma = 1.4$  keV for the **compps** models. EW: line equivalent width. Uncertainties are at the 90% confidence level for one interesting parameter ( $\Delta\chi^2 = 2.71$ ). The interstellar equivalent column was fixed at  $N_{\text{H}} = 3.2 \times 10^{20}$  cm<sup>-2</sup>. <sup>a</sup>Parameters for a broad iron line with  $\sigma = 1.4^{+0.2}_{-0.2}$  keV. <sup>b</sup>Parameters for a broad line with  $\sigma = 1.4^{+0.2}_{-0.1}$ .

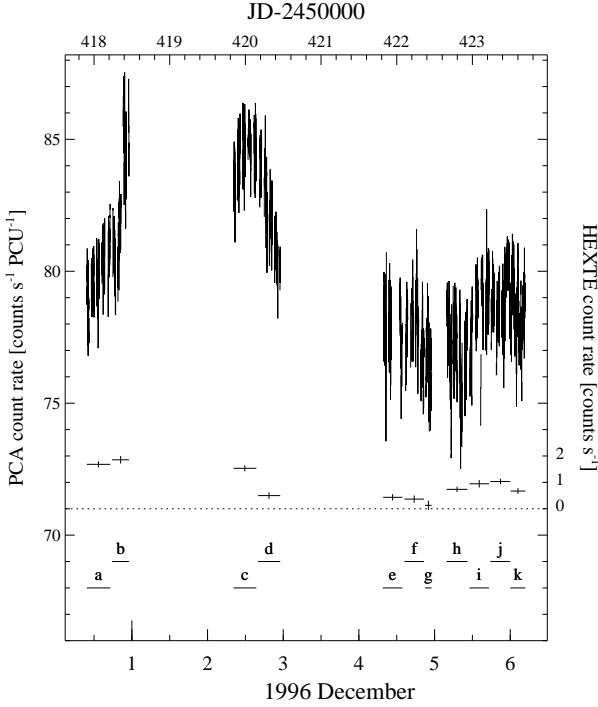


**Figure 1.** Background-subtracted *RXTE* PCA lightcurve of LMC X-3, rebinned to a resolution of 64 s (left  $y$ -axis), and total background subtracted *HEXTE* count rate (sum of *HEXTE* clusters A and B; right  $y$ -axis). The dashes indicate the individual observations of Table 1.

power-law component. We modeled absorption in the intervening interstellar medium by fixing the equivalent hydrogen column to the value found from radio observations  $N_{\text{H}} = 3.2 \times 10^{20} \text{ cm}^{-2}$  (Staveley-Smith 1999, priv. comm.), and by using the cross sections of Bałucińska-Church & McCammon (1992). Our preliminary fits to this model had strong residuals in the region around  $\sim 6.5 \text{ keV}$  (Fig. 3, middle). We therefore included a narrow emission line at 6.4 keV. We will return to the issue of the reality of this line feature below. Table 2 lists the parameters of the best fit models.

The characteristic temperature of the phenomenological accretion disc component,  $kT_{\text{in}}$ , can be determined to high accuracy (see also Paper II). The formal uncertainty of the values for  $kT_{\text{in}}$  presented in Table 2 are typically smaller than 0.005 keV. This rather small formal uncertainty value might indicate that the systematic uncertainty of the response matrix needs to be taken into account even for these short observations. These systematic uncertainties, however, are of roughly the same magnitude as the Poisson errors used in our analysis. This fact makes a formal error analysis rather difficult, and it is not clear whether the parameter error analysis methods of Lampton et al. (1976) yield meaningful results in such a case.

During the week over which the observations were performed,  $kT_{\text{in}}$  remained more stable than the other fit parameters, although these other parameters had relatively weak variations. It has been observed that on much longer time scales (months to years) variations of LMC X-3 are correlated predominantly with strong variations of  $kT_{\text{in}}$ , while

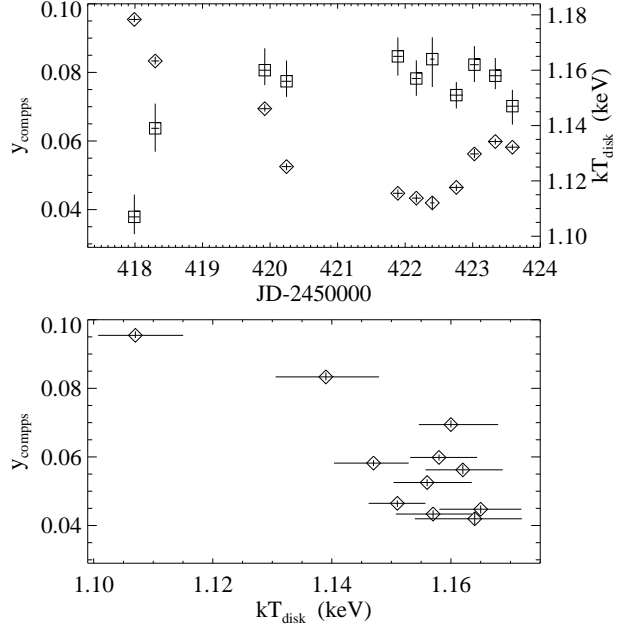


**Figure 2.** *Top:* Peak disc temperature and Compton  $y$ -parameter as a function time for the observations of LMC X-3 presented in Tab. 1. *Bottom:* Peak disc temperature vs. Compton  $y$ -parameter.

the phenomenological disc normalisation,  $A_{\text{disc}}$ , remains relatively constant (Paper II, Ebisawa et al. 1993). In the literal interpretation of the multi-temperature disc black body,  $A_{\text{disc}} \propto r_{\text{in}}^2 \cos i$ , where  $r_{\text{in}}$  is the inner radius of the accretion disc and  $i$  is its inclination. The stability of  $A_{\text{disc}}$  thus has been interpreted as evidence that the inner radius of the accretion disc stays remarkably constant on long timescales (Ebisawa et al. 1993). As discussed by Merloni et al. (1999), however, this is not necessarily true for a more physical disc model that accounts for radiative transfer effects, Doppler blurring, and gravitational redshifting. For example, a model wherein only the accretion rate and not the inner disc radius varies formally can be fit with a disc black body with varying  $A_{\text{disc}}$  (Merloni et al. 1999).

As a more physically motivated description, we have also fit the Compton scattering model of Poutanen & Svensson (1996) (**compps**). Specifically, we simulate a disc black body Compton upscattered via a slab geometry corona with fixed unity covering fraction over the disc. A purely thermal coronal electron distribution was assumed, and the width of the Fe line was fixed to be  $\sigma \sim 1.4 \text{ keV}$  (see below). We then fit the peak temperature of the disc black body, as well as the electron temperature and Compton  $y$ -parameter of the corona. Results are presented in Table 1 and in Fig. 2. Here the peak temperature of the disc is seen to vary more strongly over the course of the observation than for the multi-temperature black body plus power-law models. The variations in the lightcurve are consistent with being predominantly driven by variations of the Compton  $y$ -parameter, with the large count rate change from observations a to e corresponding to a drop in  $y$ . The slight increase in count rate seen in observations h–k corresponds to a slight increase in  $y$ . There is a tendency for the peak disc tem-

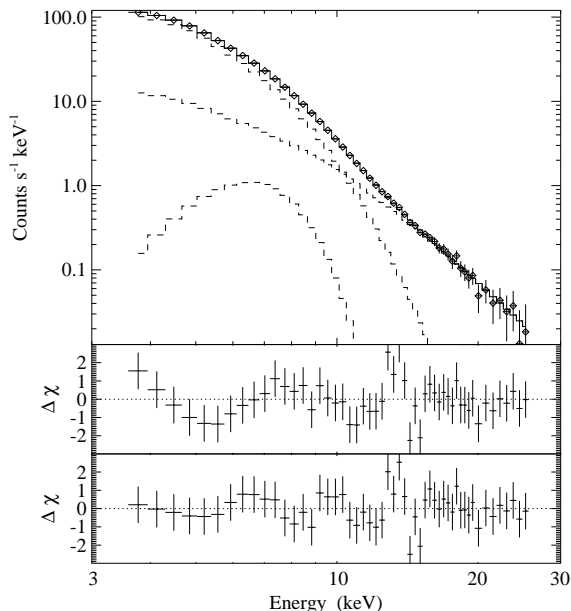


**Figure 3.** Top: Observed spectrum and disc black body plus power law plus broad iron line model fit to the long observation of LMC X-3. Dashed lines show the individual model components folded through the detector response. Middle: Residuals in units of  $\sigma$  between the data and the model, with a narrow iron line. Bottom: Residuals for the best fit model, including a very broad iron line. (Residuals for the `compps` model are virtually identical.)

perature and Compton  $y$ -parameter to be anti-correlated; however, this anti-correlation is dominated by observations a and b.

Note that the lightcurves cover approximately 3, 1.7 day orbital periods of LMC X-3. Recent work with these (now archived) *RXTE* observations, along with more recent long-term pointings, reveal evidence for a weak (few percent) orbital modulation of the X-ray source if one folds the lightcurves on the known orbital period (Boyd & Smale, in prep.). Such variations would not be unexpected as previous observations have suggested a near edge-on system to account for the ellipticity of the optical lightcurve (van der Klis et al. 1983). The nature of these variations, possibly due to weak scattering, will be discussed further by Boyd & Smale (2000).

We now consider fits to the summed spectrum from the long observation. Taking *PCA* channels 7 to 58 ( $\approx 3.6$ – $26$  keV), we again fit two models: a disc black body plus power law plus gaussian line, and a `compps` model plus gaussian line. The best fit disc black body plus power law models are shown in Fig. 3. For both classes of models, we formally required a broad Fe line component with equivalent width  $\gtrsim 150$  eV with widths of  $\sigma \approx 1.4$  keV (Table 2). This is approximately twice the *PCA* spectral resolution. Despite the low reduced  $\chi^2$ , we do not consider such a strong line to have been detected definitively in LMC X-3 as there is some concern about systematic errors in both the *PCA* response and the spectral model.

Excluding the line, residuals in the line region are  $\sim 1\%$ , similar to the systematic uncertainties in the *PCA* response. In addition, for the models that we have fit, energy channels

$\lesssim 6$  keV are dominated by the disc component, whereas energies  $\gtrsim 10$  keV are dominated by the power-law/Comptonised component. The crossover region corresponds to the Fe line region (see Fig. 3). Thus the line strength is especially sensitive to any errors in modelling the continuum spectral shape, such as, e.g., the approximation made by the `diskbb`+power model, where the comptonised spectrum is represented by a pure power-law even at energies where the comptonised photons have energies comparably to the seed photon energy. This is in contrast to AGN, for example, where the continuum through the line/edge region is thought to be reasonably well-approximated by a featureless power law, and therefore is not subject to systematic uncertainties in the continuum model.

For the case of AGN, the reality of the line can also be verified (independently of response matrix uncertainties) by taking the ratio of the (nearly power-law) observed spectrum to that of the power-law spectrum of the Crab nebula. In principle, a similar procedure could also be used in case of LMC X-3. Simulating a `compps` spectrum both with and without a line, utilizing the fit parameters for LMC X-3 discussed above, shows that a division of these two spectra would reveal the presence of a line. There exists no template spectrum, however, with which to do this comparison. We caution, therefore, that the LMC X-3 line in reality may be weaker and/or narrower than that obtained here.

The Comptonisation model implies a coronal temperature of  $\approx 60$  keV, and a Compton  $y$ -parameter of  $y \equiv 4kT_{\text{es}}/mc^2 \tau_{\text{es}} \approx 0.06$ , which implies an optical depth of  $\tau_{\text{es}} \approx 0.1$ . Due to the limited energy range of our observations, however, these fits are not unique. We assumed a purely thermal electron distribution, but we note that a purely non-thermal Comptonizing electron distribution fits the data equally well. Data at energies significantly higher than 50 keV are required to break this degeneracy.

As regards the power-law component, when considering the *HEXTE* data as well, we detect the source out to  $\approx 50$  keV, the highest energy at which this source has ever been detected. The *HEXTE* data, however, do not place much stronger constraints than were obtained with the *PCA* data alone. Including the *HEXTE* data, the observed power law is  $\Gamma = 2.8^{+0.1}_{-0.2}$ . We do not detect any noticeable curvature in the spectrum, but our limits on the presence of such curvature are weak.

### 3.2 LMC X-1

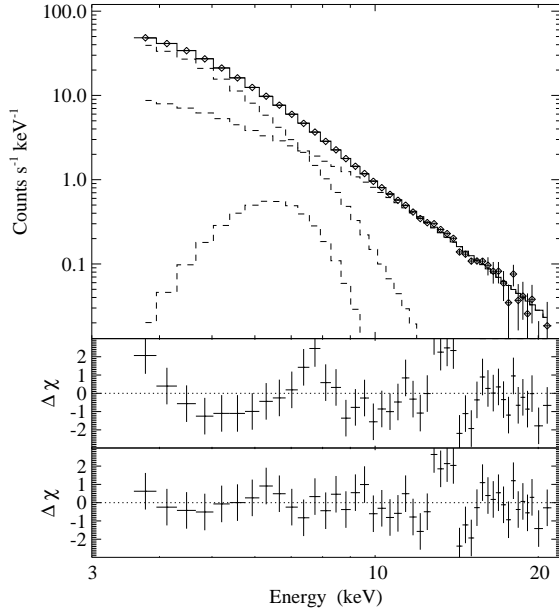
Historically, LMC X-1 has shown relatively little long time scale variability (Syunyaev et al. 1990, see also Paper II). Consistent with this, LMC X-1 showed no obvious variations on day long time scales during the long *RXTE* observation of 1996 December 6 to 8. The combined spectrum is a typical example of the spectrum of LMC X-1 (see Paper II). Taking our screening criteria into account, we obtained 80 ksec of data with 5 PCU on, and another 30 ksec of data wherein there were 3 or 4 PCU on. Again, these data have been added together as for LMC X-3. This resulted in a detection of LMC X-1 out to 20 keV in the *PCA*. In *HEXTE*, LMC X-1 is detectable out to the same energy, but due to its low count rate (the total *HEXTE* count rate is  $\lesssim 1$  counts  $\text{s}^{-1}$ ), no spectral information can be obtained.

We modeled the data (*PCA* channels 7 to 52,  $\approx 3.6$ –

**Table 3.** Results of Spectral Fitting to the LMC X-1 Data.

$kT_{\text{in}}$ keV	$A_{\text{disc}}$	$A_{\text{compps}}$ $10^{-2}$	$\Gamma$	$A_{\text{PL}}$ $10^{-1}$	$kT_e$ keV	$y_{\text{compps}}$ $10^{-2}$	$\sigma$ keV	$A_{\text{Line}}$ $10^{-5}$	EW eV	$\chi^2/\text{dof}$
$0.91^{+0.01}_{-0.01}$	$58.0^{+3.1}_{-3.0}$	...	$3.1^{+0.1}_{-0.1}$	$2.1^{+0.6}_{-0.6}$	...	...	<i>0.1</i>	$7^{+4}_{-5}$	38	71.8/41
$0.88^{+0.01}_{-0.01}$	$76.3^{+3.7}_{-6.0}$	...	$2.9^{+0.1}_{-0.1}$	$1.5^{+0.4}_{-0.5}$	...	...	$0.98^{+0.19}_{-0.15}$	$32^{+10}_{-10}$	195	46.4/40
$0.86^{+0.02}_{-0.02}$	...	$1.9^{+0.0}_{-0.3}$	...	...	$68^{+7}_{-8}$	$4.4^{+0.1}_{-0.3}$	$0.97^{+0.18}_{-0.14}$	$33^{+10}_{-9}$	207	48.5/40

See Table. 2 for an explanation of the symbols. The interstellar equivalent column was fixed at  $N_{\text{H}} = 7.2 \times 10^{21} \text{ cm}^{-2}$ . Parameters typeset in italics were frozen at the indicated value. Errors are at the 90% confidence level for one interesting parameter ( $\Delta\chi^2 = 2.71$ ).

**Figure 4.** Same as Fig. 3 for the long observation of LMC X-1.

22 keV) with the same spectral models as that for LMC X-3, using an equivalent hydrogen column of  $N_{\text{H}} = 7.2 \times 10^{21} \text{ cm}^{-2}$  (Staveley-Smith 1999, priv. comm.), taken from 21 cm measurements. Again, the data required the presence of an iron line at 6.4 keV. The resulting best fit parameters, with a narrow and with a broad iron line, are shown in Table 3. In Figure 4, we display the residuals of the disc black body fits, showing the improvement of assuming a broad iron line. As for LMC X-3, without a broad line the relative deviation between the data and the model in the line region is  $\approx 1\%$ . Again, the line region corresponds to the transition region between the disc black body and power-law/Comptonized emission components of the spectrum, so caution is warranted in interpreting the fit parameters of the line.

Our spectral parameter values are in general agreement with earlier data (Ebisawa et al. 1989; Schlegel et al. 1994), although our power-law index appears to be rather soft compared to the earlier measurements. As we show in Fig. 4, the soft ( $\Gamma \sim 3$ ) power-law component dominates the observed flux above  $\sim 7$  keV, but also contributes an appreciable fraction of the total soft flux. Thus the lower energy channels are also in part determining the value of the fitted spectral index. In terms of the *compps* Comptonisation model, if we choose a purely thermal, slab-geometry corona with unity covering factor, we find similar coronal parameters

as for LMC X-3; however, the disc temperature is somewhat lower so the observed spectrum is more dominated by Comptonized photons than that for LMC X-3. Again, purely non-thermal models are also permitted, indicating that the coronal geometry and parameters are not uniquely determined by these data.

Since our observations cover a larger energy range than many previous missions, they ensure that our best fit models at least describe the spectral shape quite well. In accordance with Schlegel et al. (1994), we do not find evidence for a broad iron edge feature in the data. Such a feature might be artificially introduced in the data for instruments where the upper energy boundary is so low that the power-law index cannot be well constrained.

#### 4 ARCHIVAL ASCA DATA

The High Energy Astrophysics Archive (HEASARC) contains one *ASCA* observation of LMC X-1 (1995 April 2) and two observations of LMC X-3 (1993 September 23, 1995 April 15). To the best of our knowledge, these observations have not been published previously. We extracted the data from all four instruments on *ASCA*, the two solid state detectors (*SIS0* and *SIS1*) and the two *GIS* detectors (*GIS2* and *GIS3*); however, here we only discuss the *SIS* data, as the *SIS* has a more reliable low energy response and a better spectral resolution.

We used the *SISCLEAN* tools (Day et al. 1998), with the default values, to remove hot and flickering pixels. Furthermore, we filtered the data with the same cleaning criteria outlined by Brandt et al. (1996); however, we took the more conservative values of  $10^\circ$  for the minimum elevation angle and  $7 \text{ GeV}/c$  for the rigidity. We obtained background estimates by extracting source-free regions near the edges of the *SIS* chips. The spectra were rebinned so that each energy bin contained a minimum of 20 photons, and we only fit *SIS* data in the 0.5 to 10 keV range. Cross-calibration uncertainties between the two *SIS* detectors were accounted for by introducing multiplicative constants (always found to be within  $\lesssim 1\%$  of each other) for each detector in all fits.

Neutral hydrogen absorption of a disc black body spectrum (Mitsuda et al. 1984) provides a rough description of the *ASCA* data. Such models yielded reduced  $\chi^2$  values  $\gtrsim 2$  for LMC X-1 and  $\approx 1$  for LMC X-3. All three observations, however, exhibited evidence for excess emission at energies  $\gtrsim 5$  keV. Adding a power law (photon flux  $\propto E^{-\Gamma}$ , with  $\Gamma \approx 2.2\text{--}2.5$ ) improved the reduced  $\chi^2$  to  $\approx 1.1$  and  $\approx 0.7$  for LMC X-1 and LMC X-3, respectively. As for the *RXTE* observations, we also were able to fit the *compps* model; how-

**Table 4.** Results of fitting the LMC X-1 and LMC X-3 ASCA data.

Source	$N_{\text{H}}$ $\times 10^{22} \text{ cm}^{-2}$	$kT_e$ keV	$A_{\text{compps}}$ $10^{-2}$	$y_{\text{compps}}$ $10^{-2}$	$kT_{\text{ray}}$ keV	$A_{\text{ray}}$ $10^{-2}$	$\chi^2/\text{dof}$
LMC X-1	$0.63^{+0.01}_{-0.01}$	$0.75^{+0.00}_{-0.01}$	$6.2^{+0.0}_{-0.0}$	$10.1^{+0.1}_{-0.4}$	...	...	498/464
(1995 Apr. 12)	<i>0.72</i>	$0.67^{+0.01}_{-0.01}$	$8.7^{+0.2}_{-0.3}$	$12.2^{+0.3}_{-0.3}$	...	...	924/465
	<i>0.72</i>	$0.71^{+0.01}_{-0.00}$	$7.2^{+0.2}_{-0.3}$	$10.9^{+0.4}_{-0.4}$	$0.82^{+0.02}_{-0.03}$	$2.5^{+0.2}_{-0.3}$	523/463
LMC X-3	$0.06^{+0.01}_{-0.00}$	$0.83^{+0.01}_{-0.00}$	$2.7^{+0.3}_{-0.0}$	$11.2^{+0.6}_{-0.5}$	...	...	295/429
(1995 Apr. 15)							
LMC X-3	$0.03^{+0.00}_{-0.01}$	$0.70^{+0.01}_{-0.01}$	$2.0^{+0.3}_{-0.2}$	$11.9^{+1.1}_{-1.0}$	...	...	231/414
(1993 Sep. 23)							

See Table. 2 for an explanation of the symbols.  $kT_{\text{ray}}$ ,  $A_{\text{ray}}$  are the temperature and normalization of the Raymond-Smith plasma component (Raymond & Smith 1977). Parameters typeset in italics were frozen at the indicated value. Errors are at the 90% confidence level for one interesting parameter ( $\Delta\chi^2 = 2.71$ ).

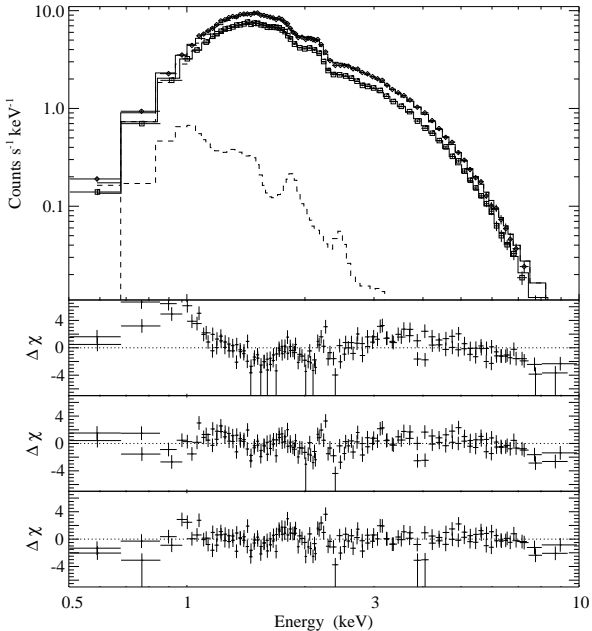


**Figure 5.** ASCA observations of LMC X-1. Top panel shows the *compps* plus a Raymond-Smith plasma model fit to the data, with  $N_{\text{H}}$  fixed to  $7.2 \times 10^{21} \text{ cm}^{-2}$ . Dashed lines show the individual model components folded through the response matrix of the *SIS0* detector. Lower panels, from top to bottom, show data residuals for: *compps* model with fixed  $N_{\text{H}}$  and no plasma component, *compps* model with fixed  $N_{\text{H}}$  and a Raymond-Smith plasma component, and *compps* model with free  $N_{\text{H}}$  and no plasma component.

ever, given that the ASCA data cuts-off at 10 keV there was not enough leverage to fit both  $kT_e$  and  $y_{\text{compps}}$ . We therefore froze the coronal electron temperature to 50 keV for all three observations. Results for these fits are presented in Table 4 and Fig. 5.

Both LMC X-3 observations are at very low flux values. We compared the 3–9 keV flux values from these observations to those obtained from our *RXTE* monitoring observations in Paper II. Using an *SIS/PCA* normalisation ratio of 0.7, we estimate that the ASCA observations would correspond

to ASM count rates of  $\sim 1.3$  cps and  $\sim 0.6$  cps. As discussed in Paper II, these low count rates occur near transitions from the soft to hard state of LMC X-3. We note that the lower flux ASCA observation of LMC X-3 shows a significant drop in peak disc temperature, consistent with the trends seen in the state transitions discussed in Paper II.

Our main purpose for examining the ASCA data is to determine if there is evidence for an Fe line in the spectrum and an Fe-L complex near energies of  $\approx 1$  keV. Line features near 1 keV are a common occurrence in photoionized plasmas close to sources emitting hard X-rays (e.g., in eclipse in Vela X-1, Nagase et al. 1994). We would also expect such features in models of warped accretion discs with winds, similar to those of Schandl (1996), or in models of wind-driven limit cycles (Shields et al. 1986), as might be relevant for producing the long term periodicity of LMC X-3 (Paper II). Such a line complex also was seen in the spectrally very similar source V1408 Aql=4U1957+11 (Nowak & Wilms 1999).

Starting with the *compps* models, none of the three ASCA observations show evidence of an Fe line. If we freeze the line energy at 6.4 keV or 6.6 keV and the line width at 0.3 keV, we find an upper (90% confidence) limit of 60 eV for the line equivalent width for the LMC X-1 observation. Narrower lines (down to the ASCA resolution of  $\sim 0.1$  keV) produce more stringent equivalent width limits. For the slightly fainter 1995 April 15 and 1993 September 23 LMC X-3 observations, the equivalent width 90% confidence limits are 90 eV and 320 eV, respectively.

The reduced  $\chi^2$  values with the *compps* model are significantly less than one for both LMC X-3 observations, and therefore we do not attempt to fit a plasma component to these data. The *compps* model fit to the LMC X-1 observation yields a reduced  $\chi^2 \approx 1$ ; however, this fit requires an  $N_{\text{H}}$  value 12% lower than the estimates of Staveley-Smith (1999, priv. comm.). Fixing the  $N_{\text{H}}$  column density to this value worsens the reduced  $\chi^2$  to  $\approx 2$  and yields significant residuals in the Fe-L complex region (Fig. 5). This residual can be removed and the reduced  $\chi^2$  value returned to  $\approx 1$  by adding a plasma component with  $kT \sim 0.8$  keV (here modeled with the XSPEC *raymond* model, after Raymond & Smith 1977). Thus the reality of any Fe-L complex is seen

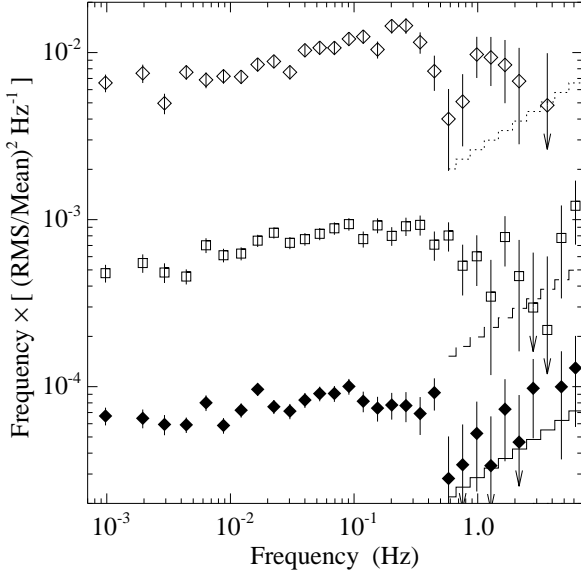


**Figure 6.** Fourier frequency times Power Spectral Density (PSD) for LMC X-1 in the 0–3.3 keV (solid diamonds, lowered by a decade), 3.3–4.7 keV (clear diamonds), 4.7–9.1 keV (solid squares, raised by a decade) energy bands. PSD normalisation is such that integrating over positive frequencies yields the mean square variability divided by the square of the mean for the lightcurve analyzed. Lines represent the expected level of positive  $1\text{-}\sigma$  noise residuals after subtracting Poisson noise from the PSDs.

to depend strongly upon accurate modeling of the neutral hydrogen absorption of this source. Differing metal abundances in the LMC also could lead to errors in interstellar absorption models, adding further uncertainties to the level of any plasma component. If real, however, a plasma component at the levels allowed by the *ASCA* data with a fixed neutral hydrogen column would be readily detectable by the X-ray Multiple Mirror Mission, which would also resolve the complex into individual line components (Note also that the residuals seen at  $\sim 1.7$  and  $\sim 2.2$  keV are likely related to well-known systematic features in the *SIS* responses matrices.)

## 5 TIMING ANALYSIS

We employed Fourier techniques, in the same manner as for our *RXTE* observations of Cyg X-1 (Nowak et al. 1999a), to study the short timescale variability of LMC X-1 and LMC X-3. Specifically, we used the same techniques for estimating deadtime corrections (Zhang et al. 1995; Zhang & Jahoda 1996) to the Power Spectral Density (PSD), and for estimating uncertainties and the Poisson noise levels of the PSD (Leahy et al. 1983; van der Klis 1989). In the analysis discussed below, we use lightcurves with  $2^{-7}$  s resolution constructed from the *PCA* top Xenon layer data only. Furthermore, we subdivide the lightcurves into three energy channels: 0–3.3 keV, 3.3–4.7 keV, and 4.7–9.1 keV (absolute *PCA* channels 0–8, 9–12, 13–24, respectively). We chose these energy ranges as they are relatively background free, and furthermore the three channels have roughly equal count

rates. The lowest energy channel is dominated by the disc component, whereas the highest energy channel is sampling the power law component (§3).

To maximize the signal to noise ratio, we created a single PSD in each energy channel that was averaged over the entire duration of our observations. We further averaged PSDs constructed from data segments of 1024 sec duration (76 segments for LMC X-1, 65 segments for LMC X-3), and we logarithmically binned the PSD over frequencies  $f \rightarrow 1.3f$ . For the case of LMC X-3, weak variability with root mean square (rms) amplitude of 0.8% of the mean was detected in the  $10^{-3}$ – $10^{-2}$  Hz range. This is consistent with background fluctuations.

Significant variability above the noise, however, was detected in LMC X-1. Root mean square variabilities of 6.5%, 6.3%, and 7.1%, lowest to highest energy channel, were found for the frequency range  $7 \times 10^{-4}$ –0.3 Hz. The PSDs for these energy channels are shown in Fig. 6. All three PSDs are approximately proportional to  $f^{-1}$  from  $7 \times 10^{-4}$ –0.2 Hz. The highest energy band PSD, however, shows evidence for a rollover at  $\sim 0.2$  Hz. Note that for this latter PSD there are only three or four points at frequencies higher than 0.2 Hz that sharply decline, followed by several points with a more gradual decline roughly proportional to  $f^{-0.5}$ . (Fig. 6 shows the PSD multiplied by frequency.) The  $f^{-0.5}$  behaviour is also readily apparent at high frequencies in the PSD of the low energy channel as well as possibly in the PSD of the middle energy channel. An  $f^{-0.5}$  proportionality is exactly that expected for positive noise residuals if the mean Poisson noise level was slightly underestimated (see Nowak et al. 1999a). The uncertainty in the noise level makes it difficult to assess the frequency-dependence of the rollover as a function of energy. The 4.7–9.1 keV energy band PSD values at frequencies 0.2–2 Hz, however, clearly lie below an extrapolation of the low-frequency PSD behaviour. Removing the break altogether would require that we *overestimated* the Poisson noise level, which seems doubtful given the  $\propto f^{-0.5}$  behaviour of the noise-subtracted PSD residuals.

These results for LMC X-1 are roughly consistent with the previous *RXTE* observations reported by Schmidtke et al. (1999) in terms of overall PSD amplitude and shape. However, Schmidtke et al. (1999) did not attempt any noise subtraction and did not search for breaks in any of the PSD. We do not find any evidence for a 0.08 Hz quasi-periodic oscillation as reported by Ebisawa et al. (1989), which is consistent with the results of Schmidtke et al. (1999). The 0.08 Hz QPO reported by Ebisawa et al. (1989), however, is nearly coincident with the expected level of the residuals after noise subtraction. Thus the previously reported QPO may have been an artifact of a misestimation of the Poisson noise level, as opposed to the lack of detection here and in the work of Schmidtke et al. (1999) being due to an intermittent nature of such low-frequency QPO.

Contrary to the results reported by Treves et al. (1988), we do not detect any variability from LMC X-3. We note, however, that the PSD reported by Treves et al. (1988) has the characteristic  $f^{-0.5}$  shape and amplitude expected from noise residuals. We believe, therefore, that the results of Treves et al. (1988) are consistent with those reported here.

We further studied the temporal behaviour of LMC X-1 by computing the Fourier frequency-dependent time lags and variability coherence between the various energy bands

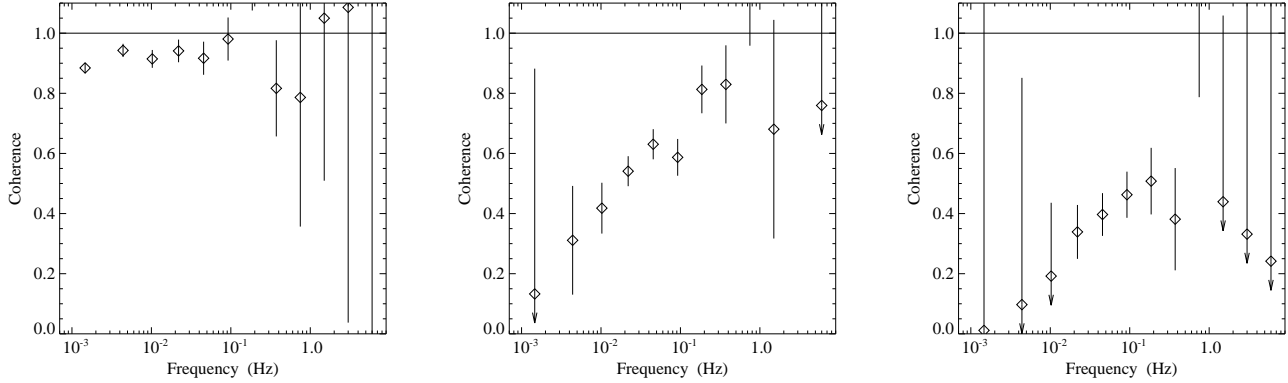


**Figure 7.** Coherence between the variability in the 0–3.3 keV and 3.3–4.7 keV energy bands (left), the 3.3–4.7 keV and 4.7–9.1 keV energy bands (middle), and the 0–3.3 keV and 4.7–9.1 keV energy bands (right).

(see Vaughan & Nowak 1997, and references therein). Due to the low count rates, only weak  $1\text{-}\sigma$  upper limits of  $\gtrsim 2 \text{ sec } (f/10^{-2} \text{ Hz})^{-1}$  could be placed on the time lags between the lowest and highest energy channels over the frequency range  $10^{-3}$ –0.3 Hz. We were able to measure the coherence among the variability in the various energy bands. As we have previously discussed (Vaughan & Nowak 1997; see also Bendat & Piersol 1986), the coherence function,  $\gamma^2(f)$ , which is always  $\leq 1$ , is a measure of the degree of linear correlation between two time series, or alternatively, it is a measure of how well one time series can be predicted from the other.

We present the coherence function for the LMC X-1 variability lightcurve, logarithmically binned over frequencies  $f \rightarrow 2f$ , in Fig. 7. The lowest and middle energy band lightcurves are fairly well-correlated and have a coherence function between them of  $\gamma^2(f) \gtrsim 0.9$ . Both of these lightcurves, however, are very incoherent with the highest energy band lightcurve, with  $\gamma^2(f) \approx 0$  at  $10^{-3}$  Hz and then rising approximately as  $\propto \log(f)$ . Due to uncertainties in the Poisson noise level there are additional systematic uncertainties above  $\approx 0.3$  Hz; however, the coherence is clearly below the near unity levels that we typically observe during the low/hard states of BHC such as Cyg X-1 and GX339-4 (Nowak et al. 1999a; Nowak et al. 1999b).

## 6 DISCUSSION

### 6.1 Variability of LMC X-1

The most obvious striking difference between LMC X-1 and LMC X-3 is that the former shows moderate (7% rms) variability whereas the latter shows essentially none ( $< 0.8\%$  rms) on timescales shorter than 1 ks, despite the fact that the X-ray spectra of these two objects are remarkably similar in terms of shape and overall flux. We hypothesize that the differences lie within their respective modes of accretion. As discussed by Cowley et al. (1983), van der Klis et al. (1983), and Cowley et al. (1994), LMC X-3 is consistent with accreting via Roche lobe overflow. One would therefore expect the accretion rate of LMC X-3 to be relatively steady (although see the discussion of the long-term periodicity presented in Paper II). LMC X-1, on the other hand, is most likely accret-

ing partly via a wind with velocity  $v_w \gtrsim 600\text{--}1100 \text{ km s}^{-1}$  (Hutchings et al. 1983; Hutchings et al. 1987). This has a number of implications for the accretion flow.

Taking a presumed mass of  $6 M_\odot$  and a wind velocity of  $600 \text{ km s}^{-1}$  (Hutchings et al. 1987), the Hoyle-Lyttleton accretion radius (Hoyle & Lyttleton 1939; Bondi & Hoyle 1944) is then

$$R_{\text{HL}} = \frac{2GM}{v_w^2} \approx 4 \times 10^{11} \text{ cm} \left( \frac{M}{6 M_\odot} \right) \left( \frac{v_w}{600 \text{ km s}^{-1}} \right)^{-2}, \quad (1)$$

which should be compared to the binary separation of  $a \sim 2.2 \times 10^{12} \text{ cm}$  given a 4.2 day period and a  $20 M_\odot$  companion (Hutchings et al. 1987). The ‘‘circularisation radius’’, however, will be much smaller, by a factor of the order  $(v_{\text{orb}}/v_w)^2$ , where  $v_{\text{orb}} \sim 260 \text{ km s}^{-1}$  is the orbital velocity. This estimate comes from assuming the accreted angular momentum per unit mass goes as  $R_{\text{HL}} \cdot v_{\text{orb}}$ , and then setting this value equal to the Keplerian value at the circularisation radius. Thus, we expect a disc circularisation radius of  $\lesssim 8 \times 10^{10} \text{ cm } (v_w/600 \text{ km s}^{-1})^{-4}$ . The disc is thus expected to be smaller than would be usual for Roche lobe overflow, perhaps substantially so. For  $v_w = 2000 \text{ km s}^{-1}$ , the expected circularisation radius is  $\sim 750 GM/c^2$ .

There is a long history of numerical simulations (Fryxell & Taam 1988; Taam & Fryxell 1988; Taam & Fryxell 1989; Benensohn et al. 1997; Ruffert 1997; Ruffert 1999) showing that wind dominated accretion inherently exhibits fluctuations in the net accretion rate onto the compact object. More recent 3-D numerical integrations (Ruffert 1997; Ruffert 1999) tend to show smaller amplitude fluctuations than earlier 2-D work (Benensohn et al. 1997); however, accretion rate fluctuations of  $\mathcal{O}(10\%)$ , in rough agreement with the observed variability, are expected. LMC X-3, being Roche lobe fed, would not be expected to exhibit these fluctuations.

A disc with a truncated outer edge may also yield an explanation of the possible rollover in the high-energy band PSD seen at  $\sim 0.3$  Hz. For  $\alpha = 0.3$ ,  $H/R \sim L/L_{\text{Edd}} \sim 0.3$ ,  $M = 6 M_\odot$ , the viscous timescale at  $R = 750 GM/c^2$  is  $\sim 20 \text{ sec}$ , which is in rough agreement with the time scale of the possible rollover. This is consistent with the idea that any accretion rate fluctuations on time scales shorter than the viscous time scale at the circularisation radius are smoothed

out as they propagate into the inner X-ray emitting regions of the disc.

As discussed above, the low variability coherence values for LMC X-1 at  $f > 10^{-3}$  Hz are unlike what we observed for the low/hard states of Cyg X-1 and GX 339-4 (Nowak et al. 1999a; Nowak et al. 1999b). We are aware of three possible ways of explaining such low values (Vaughan & Nowak 1997). First, the low and high energy bands may be completely unrelated to each other. This seems unlikely as all three energy bands exhibit a roughly  $\propto f^{-1}$  PSD with comparable amplitudes. Second, the upper energy band PSD may be related to the lower energy band PSD via a non-linear transfer function. This is a viable option, given the complicated physics of “coronal formation” and the fact that non-linear transfer functions couple power from frequencies  $f$  in one band to multiples of  $f$  in other bands (Bendat & Piersol 1986). This latter case is especially difficult to detect in the  $f^{-1}$  PSD because of its scale-free nature.

The third possibility is perhaps the most viable option. “Mixing” of *independent* components with widely varying intrinsic time lags can lead to the loss of coherence (see the discussion presented by Nowak et al. 1999b). For example, if one component which shows a correlation between hard and soft X-rays (e.g., local dynamical time scale disc fluctuations leading to and increase in both seed photons and, very slightly delayed, upscattered hard photons) is mixed with another, nearly equal in power *but independent* component with an anti-correlation between soft and hard X-rays (e.g., matter being transferred between disc and corona on thermal or viscous time scales, with comparably long delays between soft and hard photons), then a strong loss of coherence is expected. In a simple two-component model the coherence function,  $\gamma^2(f)$ , is given by

$$\gamma^2(f) \approx \frac{R^2(f) + 2R(f) \cos(\theta_b - \theta_a)}{[R(f) + 1]^2}. \quad (2)$$

Here  $R(f)$  is the ratio of Fourier frequency-dependent cross correlation amplitudes for the two independent processes being considered (soft vs. hard X-ray variability, process  $b$  over process  $a$ ), and  $\theta_a$ ,  $\theta_b$  are the Fourier frequency-dependent phase delays between the hard and soft X-ray variability for the independent processes  $a$  and  $b$ , respectively (Vaughan & Nowak 1997; Nowak et al. 1999b). (Time delay,  $\tau \equiv \theta/2\pi f$ .) For the plots in Fig. 7, if  $R(f) \approx 1$  and  $\theta_b - \theta_a \approx \pi$  at  $f = 10^{-3}$  Hz, then  $\gamma^2(f) \approx 0$  there as well. The increase in coherence towards higher frequency could be due to a decrease of either  $\theta_b - \theta_a$  or  $R(f)$ . The latter might be reasonably expected, for instance, if one process is happening predominantly on  $\mathcal{O}(1000 \text{ sec})$  viscous time scales (again, perhaps matter/energy transfer between disc and corona), whereas the other one is happening over a broader range of time scales (fluctuations in the seed/Comptonized photons).

## 6.2 Spectroscopy of the Soft State

The spectroscopy of LMC X-3 perhaps bears out the notion of there being an anti-correlation between the disc and coronal components on long time scales, as shown in Fig. 2. A similar result can be obtained with the more phenomenological disc black body plus power law models presented in Table 2. The photon flux in the ‘disc component’ ( $\propto A_{\text{disc}} k T_{\text{disc}}^3$ ) is anti-correlated with the photon flux in

the ‘power law component’ ( $\propto 3.6^{1-\gamma}/[1-\gamma]$ ) in an analogous way. The fastest variation occurs on time scales of  $\approx 0.4$  days. Given  $\alpha = 0.3$ ,  $H/R \sim L/LEdd \sim 0.3$ , and  $M = 9 M_{\odot}$ , this corresponds to a viscous time scale at a radius of  $\sim 8 \times 10^{10}$  cm, approximately one quarter of the disc circularisation radius. It is therefore more likely that this variation occurs on a thermal or dynamical time scale closer towards the center of the system. Thermal time scale transfer of energy between disc and corona is again consistent with the results shown in Fig. 2.

Unfortunately, it is difficult to say much more about the spectrum other than it is well-fit by a disc black body plus power law model. Given a  $70^\circ$  inclination,  $9 M_{\odot}$  black hole, and 50 kpc distance for LMC X-3, and a  $30^\circ$  inclination,  $6 M_{\odot}$  black hole, and 50 kpc distance for LMC X-1, the disc normalisations in Tables 2 and 3 are roughly consistent with inner disc radii of  $\sim 6 GM/c^2$ . This is quite remarkable, given the simplicity of the disc black body model (cf., Merloni et al. 1999). As regards the power law tail, other soft state black hole candidates exhibit evidence for non-thermal Comptonisation in this tail (Gierliński et al. 1999). Here, however, as we were only able to go out to 50 keV and 20 keV for LMC X-3 and LMC X-1, respectively, we were able to describe the data completely adequately with pure thermal Comptonisation.

The extent to which a strong, broad Fe line is required is likewise still somewhat uncertain. The  $\approx 150$  eV equivalent width,  $\sigma \approx 1.4$  keV line is consistent with expectations from the basic picture outlined above: a disc extending down towards the black hole horizon, with a large covering fraction corona sitting on top of it. (A slight Fe overabundance, or perhaps beaming of the coronal radiation towards the disc might also be required for the implied equivalent widths.) However, as the Fe line occurs in a region where the two basic spectral components — soft disc spectrum and hard power law/Comptonisation spectrum — cross one another, the Fe line parameters are especially sensitive to our assumptions regarding the underlying continuum model. Again, this is in contrast to AGN where it is presumed that the underlying continuum in the Fe line/edge region is well-approximated by a simple power law.

## 7 SUMMARY

In this work, we have presented analysis of long (170 ksec) *RXTE* observations of LMC X-1 and LMC X-3, as well as analysis of archival *ASCA* observations of these objects. The primary results of these analyses are as follows.

- Both LMC X-1 and LMC X-3 are well-fit by a simple spectroscopic model consisting of a disc black body and a power law. The power law, which was seen out to 50 keV for LMC X-3, shows no obvious curvature. The data are consistent with exhibiting a broad Fe  $K\alpha$  line with equivalent width  $\lesssim 150$  eV; however, the line could in reality be narrower and weaker. *ASCA* observations do not reveal the presence of a narrow Fe  $K\alpha$  line, and the presence of any Fe L-complex in LMC X-1 is almost completely dependent upon the modeling of the neutral hydrogen column towards that source.
- As a more physical interpretation of these results, the

spectra are consistent with Comptonisation of a disc spectrum by a corona with electron temperature  $kT_e \sim 60$  keV and  $\tau_{es} \sim 0.1$ . These fits are not unique, however, as the data do not extend beyond 50 keV. Purely non-thermal Comptonisation models are also permitted.

- LMC X-3 shows no variability on  $\lesssim 1$  ks time scales; however, it does show variability on half day time scales and longer. The time scale of these variations are slightly faster than the viscous time scales of the outer disc. Spectral models of these variations are consistent with an anti-correlation between the disc and Compton corona components of the spectrum

- LMC X-1 shows rms variability of a few percent on faster than 1000 s timescales. This variability, along with with a possible power spectrum rollover on time scales  $\lesssim 5$  s, is consistent with accretion rate variations in a wind fed system where the disc is circularized at radii  $\lesssim 1000 GM/c^2$ .

- The variability at energies  $\lesssim 5$  keV shows very low coherence with the variability at energies  $\gtrsim 5$  keV. Given the the similarity of the PSD among the three energy bands, this low coherence is likely either due to a non-linear relationship between the soft and hard energy bands, or due to multiple variability components some with strong correlations between soft and hard variability and other others with strong anti-correlations.

## ACKNOWLEDGEMENTS

This research has been financed by NASA grants NAG5-3225, NAG5-4621, NAG5-4737, NSF grants AST95-29170, AST98-76887, DFG grant Sta 172/22, and a travel grant to J.W. and K.P. from the DAAD. L. Staveley-Smith provided us with the unpublished  $N_H$  values. MAN and JW would like to thank the hospitality of the Aspen Center for Physics and the participants of the “X-ray Probes of Relativistic Astrophysics” workshop, especially J. Grindlay and R Taam, for many useful discussions while this work was being completed. We thank the referee for comments that improved the clarity of this paper.

## REFERENCES

Arnaud K.A., 1996, in Jacoby J.H., Barnes J., eds, *Astronomical Data Analysis Software and Systems V*. Astron. Soc. Pacific, Conf. Ser. 101 Astron. Soc. Pacific, San Francisco, p. 17

Balućićska-Church M., McCammon D., 1992, *ApJ*, 400, 699

Bendat J., Piersol A., 1986, *Random Data: Analysis and Measurement Procedures*, Wiley, New York

Benensohn J.S., Lamb D.Q., Taam R.E., 1997, *ApJ*, 478, 723

Bondi H., Hoyle F., 1944, *MNRAS*, 104, 273

Bowyer S., Byram E.T., Chubb T.A., Friedman H., 1965, *Science*, 147, 394

Brandt W.N., Fabian A.C., Dotani T., et al., 1996, *MNRAS*, 283, 1071

Cowley A.P., Crampton D., Hutchings J.B., 1978, *AJ*, 83, 1619

Cowley A.P., Crampton D., Hutchings J.B., et al., 1983, *ApJ*, 272, 118

Cowley A.P., Schmidtke P.C., Anderson A.L., McGrath T.K., 1995, *PASP*, 107, 145

Cowley A.P., Schmidtke P.C., Ebisawa K., et al., 1991, *ApJ*, 381, 526

Cowley A.P., Schmidtke P.C., Hutchings J.B., Crampton D., 1994, *ApJ*, 429, 826

Cui W., Zhang S.N., Focke W., Swank J.H., 1997, *ApJ*, 484, 383

Day C., Arnaud K., Ebisawa K., et al., 1998, *The ASCA Data Reduction Guide*, Technical report, NASA Goddard Space Flight Center, Greenbelt, Md. Version 2.0

Dove J.B., Wilms J., Nowak M.A., et al., 1998, *MNRAS*, 298, 729 (paper I)

Ebisawa K., Makino F., Mitsuda K., et al., 1993, *ApJ*, 403, 684

Ebisawa K., Mitsuda K., Inoue H., 1989, *PASJ*, 41, 519

Fryxell B.A., Taam R.E., 1988, *ApJ*, 335, 862

Gierliński M., Zdziarski A.A., Poutanen J., et al., 1999, *MNRAS*, 309, 496

Grebenev S., Sunyaev R., Pavlinsky M., et al., 1993, *A&AS*, 97, 281

Hoyle F., Lyttleton R.A., 1939, *Proc. Cam. Phil Soc.*, 35, 405

Hutchings J.B., Crampton D., Cowley A.P., 1983, *ApJ*, 275, L43

Hutchings J.B., Crampton D., Cowley A.P., et al., 1987, *AJ*, 94, 340

Jahoda K., Swank J.H., Giles A.B., et al., 1996, in Siegmund O.H., ed, *EUV, X-Ray, and Gamma-Ray Instrumentation for Astronomy VII*. Proc. SPIE 2808 SPIE, Bellingham, WA, p.59

Lampton M., Margon B., Bowyer S., 1976, *ApJ*, 208, 177

Leahy D.A., Darbro W., Elsner R.F., et al., 1983, *ApJ*, 266, 160

Long K.S., Helfand D.J., Grabelsky D.A., 1981, *ApJ*, 248, 925

Merloni A., Fabian A.C., Ross R.R., 1999, *MNRAS*, 313, 193

Mitsuda K., Inoue H., Koyama K., et al., 1984, *PASJ*, 36, 741

Miyamoto S., Kitamoto S., Iga S., et al., 1994, *ApJ*, 435, 398

Nagase F., Zylstra G., Sonobe T., et al., 1994, *ApJ*, 436, L1

Nowak M.A., 1995, *PASP*, 107, 1207

Nowak M.A., Vaughan B.A., Wilms J., et al., 1999a, *ApJ*, 510, 874

Nowak M.A., Wilms J., Dove J.B., 1999b, *ApJ*, 517, 355

Nowak M.A., Wilms J., 1999, *ApJ*, 522, 476

Nowak M.A., Wilms J., Vaughan B.A., et al., 1999c, *ApJ*, 515, 726

Poutanen J. & Svensson R., 1986, *ApJ*, 470, 249

Raymond, J. C., & Smith, B. W., 1977, *ApJS*, 35, 419

Rothschild R.E., Blanco P.R., Gruber D.E., et al., 1998, *ApJ*, 496, 538

Ruffert M., 1997, *AJ*, 317, 793

Ruffert M., 1999, *AJ*, 346, 861

Schandl S., 1996, *A&A*, 307, 95

Schlegel E.M., Marshall F.E., Mushotzky R.F., et al., 1994, *ApJ*, 422, 243

Schmidtke P.C., Ponder A.L., Cowley A.C., 1999, *AJ*, 117, 1292

Shields G.A., McKee C.F., Lin D.N.C., 1986, *ApJ*, 306, 90

Sunyaev R.A., Gil’fanov M., Churazov E., et al., 1990, *Sov. Astron. Lett.*, 16, 55

Taam R.E., Fryxell B., 1988, *ApJ*, 327, L73

Taam R.E., Fryxell B., 1989, *ApJ*, 339, 297

Tanaka Y., Lewin W.H.G., 1995, *Black-hole binaries*. in Lewin W.H.G., van Paradijs J., van den Heuvel E.P.J., eds, *X-Ray Binaries*. Cambridge Univ. Press, Cambridge, Ch. 3, p. 126

Treves A., Belloni T., Chiapetti L., et al., 1988, *ApJ*, 325, 119

Treves A., Belloni T., Corbet R.H.D., et al., 1990, *ApJ*, 364, 266

van der Klis M., 1989, in Ögelman H., van den Heuvel E.P.J., eds, *Timing Neutron Stars*. NATO ASI C262 Kluwer, Dordrecht, p.27

van der Klis M., Tjemkes S., van Paradijs J., 1983, *A&A*, 126, 265

Vaughan B.A., Nowak M.A., 1997, *ApJ*, 474, L43

Wilms J., Nowak M.A., Dove J.B., et al., 1999a, *ApJ*, 522, 460

Wilms J., Nowak M.A., Dove J.B., et al., 1999b, in Aschenbach B., Freyberg M., eds, *Highlights in X-ray Astronomy*. MPE Report 272, p. 98

Wilms J., Nowak M.A., Dove J.B., et al., 1999c, *Astrophys. Lett. Comm.*, 38, 273

- Wilms J., Nowak M.A., Heindl W.A., et al., 1999d, MNRAS submitted (Paper II)
- Zhang S.N., Cui W., Harmon B.A., et al., 1997, ApJ, 477, L95
- Zhang W., Jahoda K., 1996, Deadtime Effects in the PCA, Technical report, NASA GSFC, Greenbelt
- Zhang W., Jahoda K., Swank J.H., et al., 1995, ApJ, 449, 930